

# Towards multi-messenger observations of core-collapse supernovae harboring choked jets

A. Zegarelli<sup>1</sup>, D. Guetta<sup>2</sup>, S. Celli<sup>3,4</sup>, S. Gagliardini<sup>2,3</sup>, I. Di Palma<sup>3,4</sup>, and I. Bartos<sup>5</sup>

<sup>1</sup> Ruhr University Bochum, Faculty of Physics and Astronomy, Astronomical Institute (AIRUB), Universitätsstraße 150, 44801 Bochum, Germany

<sup>2</sup> Department of Physics, Ariel University, Ariel, Israel

<sup>3</sup> Istituto Nazionale di Fisica Nucleare, Sezione di Roma, P. le Aldo Moro 2, I-00185 Rome, Italy

<sup>4</sup> Dipartimento di Fisica dell'Università La Sapienza, P. le Aldo Moro 2, I-00185 Rome, Italy

<sup>5</sup> Department of Physics, University of Florida, Gainesville, FL 32611-8440, USA

March 26, 2024

## ABSTRACT

**Context.** Over the last decade, choked jets have attracted particular attention as potential sources of high-energy cosmic neutrinos. Testing this hypothesis is challenging because of the missing gamma-ray counterpart, hence the identification of other electromagnetic signatures is crucial. A choked-jet source is expected harboring in core-collapse supernovae with extended hydrogen envelopes, leading to the release of ultraviolet and optical emission for a few days. Although ultraviolet measurements of core-collapse supernovae have lagged over the years behind those in the optical band, these will increase in the next few years thanks to new instruments sensible at ultraviolet wavelengths.

**Aims.** The ultraviolet band will be visible with an unprecedentedly large field of view by the future mission satellite ULTRASAT, for which we investigate the detection prospects in relation to the choked source visibility in the optical band with the currently operating telescope ZTF. As these sources can produce neutrinos via hadronic and photohadronic interactions in choked jets, we also investigate how neutrino observations by existing Cherenkov high-energy neutrino telescopes (as IceCube and KM3NeT) can be used in association with electromagnetic signals coming from shock breakout events.

**Methods.** By considering fiducial parameters of the source population and instruments' performances, we estimate the maximum redshift up to which ULTRASAT and ZTF are able to detect ultraviolet and optical signals from these explosions, respectively. Furthermore, we discuss coordinated multi-messenger observations among those instruments and high-energy neutrino telescopes.

**Results.** ULTRASAT will be able to double the volume of sky currently visible by ZTF for the same emitting sources enlarging the sample of observed Type II supernovae by  $\sim 60\%$ . For optimized multi-messenger detections, the delay between neutrino produced at the shock breakout occurrence (during the jet propagation inside the stellar envelope) and ULTRASAT observations should be of  $\sim 4(5)$  days, with a subsequent follow-up by instruments like ZTF about one week after.

**Key words.** surveys - methods: observational - astroparticle physics - (stars:) supergiants - (stars:) supernovae: general - stars: jets

## 1. Introduction

At the end of its life, a massive star (initial mass  $> 8$  solar masses) will typically collapse into a compact object – a black hole or a neutron star. Accretion by this compact object then in turn can drive an energetic relativistic outflow, or jet. The core collapse of massive stars that are stripped of their outer layers of hydrogen and helium by strong winds produce Type Ib/c supernovae (SNe). If these outer layers are not lost, core collapse results in a Type II SN.

For Wolf-Rayet (WR) stars, i.e., very massive stars with strong winds blowing out most of the stellar envelope, the relativistic jet driven by the central compact object can easily break through the remaining stellar envelope and produce  $\gamma$ -ray emission, usually observed as a burst lasting from a few to thousands of seconds; these phenomena are called long gamma-ray bursts (LGRBs). LGRBs are typically observed together with Type Ib/c SNe but not Type II SN, suggesting that the loss of the outer stellar envelope is important for the jet's ability to escape (see e.g.,

Woosley & Bloom 2006 for a review about GRB-SN connection).

Type II SNe are associated to extended massive stars, such as blue supergiant (BSG) and red supergiant (RSG). In particular, hydrogen-rich SNe II are firmly associated with RSGs, while rare under luminous SNe II may arise from BSGs (e.g., SN 1987A (Arnett et al. 1989)). The latter may be the progenitors of the so-called ultra-long GRBs (ULGRBs), which are characterized by a  $\gamma$ -ray emission lasting  $\gtrsim 10^4$  seconds (Perna et al. 2018), thought to be generated by the fallback accretion from the extended stellar envelope (Quataert & Kasen 2012; Wu et al. 2013; Nakauchi et al. 2013). Their large radial extension constitutes a challenge to the emergence of the jet (Perna et al. 2018) as preserving a large stellar envelope (a few tens of  $R_\odot$ ) might lead to choked jets in case the central engine activity stops early enough before the jet reaches the outer edge of the star; if so,  $\gamma$ -ray emission would not emerge because of the thickness of the surrounding material. Simulations show that stellar envelopes of non-rotating RSG stars are expected to be even larger (between  $\sim 200 R_\odot$  and  $\sim 1500 R_\odot$ ; e.g., Goldberg & Bildsten 2020). This causes a very long accretion timescale ( $\sim 10^5 - 10^6$  s) and a small accretion rate of material around the central engine (e.g., Perna

\* E-mail: angela.zegarelli@astro.ruhr-uni-bochum.de

et al. 2018); because of that, there may not be enough power to launch a jet with a luminosity able to burrow through the envelope of a RSG.

In addition to the relativistic jet producing the GRB prompt emission, a *cocoon* is also expected to form by the jet depositing energy in the stellar envelope (MacFadyen & Woosley 1999). This is expected to be a comparable amount of energy to that of the prompt emission. As the GRB jet carves its way through the stellar envelope, it dissipates its energy in a double shock (forward-reverse) structure that forms at its head (Matzner 2003; Lazzati & Begelman 2005; Bromberg et al. 2011). The hot head material spills sideways, forming a cocoon that engulfs the jet and collimates it.

The first cocoon was observed in the long GRB 171205A (Izzo et al. 2019), which occurred at the unusually small distance of 163 Mpc. Detailed, multi-epoch spectroscopic observation of the associated SN 2017iuk allowed the identification of the cocoon emission as an additional black-body component of the light curve,  $\sim 1$  day after the GRB occurrence. Spectroscopic observations of the early-time SN spectrum revealed sub-relativistic material ( $v \sim c/3$ ) rich in Fe and Ni, indicating that the observed component comes from the inner depth of the star. The implications of the presence of the cocoon, as well as more details about the theoretical framework related to it, are discussed in Nakar & Piran (2017).

A choked jet dissipates all its energy within the stellar envelope and does not produce a GRB. In other words,  $\gamma$ -ray emission from the aforementioned progenitors is absorbed, hence  $\gamma$  rays associated with RSG and BSG stars cannot be caught outside of it. If before stalling the jet crosses a large fraction of the stellar envelope, the cocoon can be energetic enough to break out of the star by itself and produce an observable electromagnetic signature: a first bright X-ray/UV flash, lasting from few seconds to fractions of hour, followed by a long-lasting (day timescale) UV/O emission related to the expanding cocoon envelope. In any case, the electromagnetic signal requires the shock to reach the stellar surface. The interested reader can refer to, e.g., Waxman & Katz 2017 for details about the shock breakout (SBO) theory. On the other hand, prior to the electromagnetic emission, high-energy neutrinos may also be produced by the hidden jet: hadronic acceleration and subsequent interaction with the intense radiation field produced in the SN explosion lead to neutrinos at TeV scale that are immediately released (Mészáros & Waxman 2001). On the contrary, emitted  $\gamma$  rays in the jet are likely absorbed in pair production processes because of the presence of intense radiation fields intrinsic to the source. Note that, in such a framework, high-energy neutrinos arise from a different process with respect to that responsible for thermal MeV neutrinos produced at the core of collapsing stars, e.g., via electron-captor and pair annihilation, in a timescale of  $O(10)$  s from the core bounce (see, e.g., Tamborra & Murase 2018 for a review on neutrino production from supernovae). Neutrinos from choked jets are characterized by higher energies, are described by a non-thermal spectrum, and are emitted at later times. The TeV-PeV neutrino signal from choked jets has been considered recently by several authors (Bartos et al. 2012; He et al. 2018; Senno et al. 2018; Esmaili & Murase 2018; Fasano et al. 2021; Chang et al. 2022). In the presence of a sufficiently dense medium, also  $pp$  collisions can occur, generating further neutrinos via mesons and muon decay.

In this work we aim at investigating the capability to follow-up SBO transients generated by choked jets embedded in BSG and RSG stars with current and future facilities, via a multi-messenger approach allowing the community to combine neu-

tirino, optical, and UV data. Defining a proper follow-up strategy between these messengers could be the key for enabling the breakthrough discovery of the astrophysical sources responsible for some of the observed cosmic neutrinos. The inconsistency between the cosmic neutrino flux and the isotropic  $\gamma$ -ray background observed by the *Fermi* satellite point indeed towards hidden sources as plausible contributors. In fact, if the entirety of neutrino sources were transparent to energetic photons, the expected  $\gamma$ -ray flux would exceed the diffuse extra-Galactic flux observed by *Fermi-LAT*, requiring at least some neutrino sources to be opaque to  $\gamma$  rays (Ackermann et al. 2015; Murase et al. 2016). In addition, improved observations and analysis of choked jets can shed new light on the dynamics and evolutionary path of exploding massive stars. If all SNe are accompanied by a SBO, detecting SBO transients and their signatures might be used to reveal the properties of SN progenitors. E.g., UV observations from core-collapse supernovae (CCSNe) are expected to better constrain physical stellar properties such as progenitor radius, surface composition, and explosion energy per unit mass (Ganot et al. 2016).

The paper is organized as follows. In Section 2, we review the main features of the model under investigation, including RSGs and BSGs. In Section 3, we describe the methodology we developed for assessing the detectability of UV signals from their choked jets, presenting the results we obtain. In Section 4, we discuss the implementation of a multi-messenger framework tailored to maximising the observation prospects. Finally, we derive conclusions in Section 5. Throughout, we adopt the standard flat  $\Lambda$ -Cold Dark Matter ( $\Lambda$ CDM) cosmology with  $\Omega_m = 0.3$ ,  $\Omega_\Lambda = 0.7$ , and  $H_0 = 70 \text{ km s}^{-1} \text{ Mpc}^{-1}$ .

## 2. UV/O emission in shock breakout flares

The first electromagnetic emission escaping an exploding star emerges as a fast shock-breakout flare, with a spectrum peaking in the UV and X-ray bands. After the breakout, the stellar envelope expands and cools. As the photosphere penetrates into the outer shells of the envelope, the adiabatically cooled radiation stored within the envelope escapes, leading to early UV/O emission over a time scale of days. Several analytic and numerical solutions have been developed that are capable to model the emission at early times, i.e.,  $< 3$  hours post explosion (e.g., Nakar & Sari 2010; Sapir et al. 2013), as well as at later times (days after the explosion) (Rabinak & Waxman 2011).

RSG, BSG, and WR stars differ greatly in their UV peaks, making early UV observations a strong discriminator among progenitor classes (see Figure 1 in Ganot et al. 2016). Since in this work we focus on choked jets, we limit the discussion here to RSGs and BSGs, both characterized by Hydrogen (H)-dominated envelopes; WR stars with a He- or C/O dominated envelopes, instead, lose their Hydrogen envelope allowing the jet to break out through the star (see Sec. 1). In the present work, we adopt as a model describing the UV/O cooling signal produced after the explosion the one developed by Waxman et al. (2007), whose description is provided in the next Section.

### 2.1. A simplified model for H-dominated envelopes

In H-dominated stellar envelopes characterized by an adiabatic flow below the photosphere, the radius  $r_{\text{ph}}$  and the effective temperature  $T_{\text{ph}}$  of the photosphere penetrating into the outer shells

of the envelope are given by (Rabinak & Waxman 2011):

$$r_{\text{ph}}(t) = \begin{cases} 3.3 \times 10^{14} f_{\rho}^{-0.062} \frac{E_{51}^{0.41} t_{0.34}^{0.093}}{(M/M_{\odot})^{0.31}} t_5^{0.81} \text{ cm} & (n = 3/2), \\ 3.3 \times 10^{14} f_{\rho}^{-0.036} \frac{E_{51}^{0.39} t_{0.34}^{0.11}}{(M/M_{\odot})^{0.28}} t_5^{0.78} \text{ cm} & (n = 3), \end{cases} \quad (1)$$

and

$$T_{\text{ph}}(t) = \begin{cases} 1.6 f_{\rho}^{-0.037} \frac{E_{51}^{0.027} R_{13}^{1/4}}{(M/M_{\odot})^{0.054} t_{0.34}^{0.28}} t_5^{-0.45} \text{ eV} & (n = 3/2), \\ 1.6 f_{\rho}^{-0.022} \frac{E_{51}^{0.016} R_{13}^{1/4}}{(M/M_{\odot})^{0.033} t_{0.34}^{0.27}} t_5^{-0.47} \text{ eV} & (n = 3), \end{cases} \quad (2)$$

respectively, under the assumption that the photon diffusion is negligible. The effect of photon diffusion, so far discarded, has been estimated by Rabinak & Waxman (2011), which derived the radius above which diffusion affects the flow significantly and estimated how much the temperature and the luminosity are affected by the approximation considered in Waxman et al. (2007); as a small difference with respect to the model described above emerged, namely  $\sim 1\% - 5\%$ , we decide to neglect this effect. In previous equations,  $k = 0.34 k_{0.34} \text{ cm}^2 \text{ g}^{-1}$  is the opacity of the stellar envelope,  $E = 10^{51} E_{51} \text{ erg}$  is the kinetic energy released at the SN explosion,  $t = 10^5 t_5 \text{ s}$  is the time from the SBO, and  $f_{\rho}$  is a numerical factor of order unity that depends on the inner envelope structure and that is linearly related to the density profile of a polytropic envelope. This latter quantity scales linearly with the progenitor mass and can be described by a power-law with index  $n = 3$  for radiative envelopes typical of BSGs, and  $n = 3/2$  for efficiently convective envelopes typical of RSGs. Here we consider a stationary and uniform opacity, that applies for example to Thomson scattering dominated opacity with constant ionization, as in fully ionized hydrogen-dominated envelopes where  $k = 0.34 \text{ cm}^2 \text{ g}^{-1}$ . Parameters in Eq. (1) and Eq. (2) have a strict relation with the expected specific intensity in UV and O wavelengths. This latter is given by a black-body radiation (BB) as modified by extinction, namely the absorption and scattering of electromagnetic radiation by dust and gas intervening along the line of sight, yielding:

$$f_{\lambda}(\lambda, t) = \left( \frac{r_{\text{ph}}}{D_L(z)} \right)^2 \sigma T_{\text{ph}}^4 \frac{T_{\text{col}}}{hc} g_{\text{BB}}(x) e^{-\tau_{\lambda}}, \quad (3)$$

where  $D_L(z)$  is the luminosity distance of the source dependent on redshift  $z$ ,  $T_{\text{col}}$  is the color temperature, i.e., the temperature at which a BB would emit radiation of the same color as the given source,  $\tau_{\lambda} \equiv \tau(\lambda)$  is the optical depth at a given wavelength  $\lambda$ ,  $\sigma$  is the Stefan–Boltzmann constant,  $h$  is the Planck constant,  $c$  the speed of light in vacuum, and

$$g_{\text{BB}}(x) = \frac{15}{\pi^4} \frac{x^5}{e^x - 1} \quad (4)$$

with  $x = hc/\lambda T_{\text{col}}$ . Starting from Equation (3), the light curve visible in UV can be expressed as

$$L_{\text{UV}}(t) = 4\pi D_L^2(z) \int_{\lambda_{\text{min}}}^{\lambda_{\text{max}}} f_{\lambda}(\lambda, t) d\lambda. \quad (5)$$

By using representative values for the photospheric radius and temperature of stellar progenitors (in Equations (1) and (2), respectively), we are able to estimate the intensity of UV light emitted at a given time from the SBO and, hence characterise the corresponding light curves.

It is worth noticing that the simplified model from Waxman

et al. (2007) is valid in a Thomson scattering dominated regime, namely at early times after the SBO. It has been extended by Rabinak & Waxman (2011) to take into account that recombination taking place in stellar envelopes after about 1 day, when  $T_{\text{ph}}$  decreases down below  $\sim 1 \text{ eV}$ . Moreover, Waxman et al. (2007) introduced a more realistic characterization of the opacity (including its time dependency) as modified by recombination, thus obtaining a more accurate description of the early UV/O emission produced in SBO phenomena. However, for H-dominated envelopes the difference in the values of photospheric temperature obtained by the two methods is contained within 10% for  $T_{\text{ph}} > 1 \text{ eV}$ . As such, we decided to adopt the model of Waxman et al. (2007) neglecting any complications related to recombination processes.

### 3. Detection of shock breakout electromagnetic signals from CCSNe

With the launch of the *Neil Gehrels Swift Observatory* (Gehrels et al. 2004) in 2005, a large amount of data of CCSN light curves at peak emission was collected, thanks to its rapid slewing capabilities, space-based nature, and frequency coverage in X-ray and O/UV. Since then, the number of observed SBO events has dramatically increased, opening a new window for early SN observations, i.e., right after the massive progenitors explosion (e.g., Modjaz et al. 2009; Roming et al. 2010; Huang et al. 2018; Pritchard et al. 2014). These observations have been often associated to further detections made in the UV, visible, and near-infrared regions of the electromagnetic spectrum, e.g., by the Hubble Space Telescope (HST) (Williams et al. 2018) in the optical domain, and the Galaxy Evolution Explorer (GALEX) satellite in UV wavelengths (Ganot et al. 2016, 2022). Joint studies have allowed the astronomical community to improve the characterization of CCSNe light curves, including the signatures of SBOs. In this regards, GALEX was a pioneering project: after the very first observations of SBOs from Type II SNe in 2008 (*SNLS-04D2dc* and *SNLS-06D1jd*, Gezari et al. (2008)) through the combination of its UV data with optical observations from other instruments, it further allowed the astronomical community to increase the sample of CCSNe detected in both O and UV wavelength band, and thus possibly coming from SBO events (see e.g., in Ganot et al. (2022)).

The growing field of multi-messenger (MM) astrophysics enables to increase the detection prospects of choked jets (that are invisible to  $\gamma$  rays), through the additional inclusion of neutrino observatories. The association of a neutrino emission with O/UV signals could be crucial to probe the contribution of choked jets embedded in CCSNe to the diffuse flux of high-energy astrophysical neutrinos observed since more than ten years to date (IceCube Collaboration 2013; Aartsen et al. 2013). While  $\gamma$  rays are commonly adopted for joint studies of astrophysical sources with neutrino data, due to a potential common hadronic origin, for hidden sources instead it appears crucial to establish an alternative strategy profiting of signatures at other wavelengths. It is worth noticing that to date, optical and X-ray follow-up program searches for such transient sources have been performed as a result of alerts from neutrino telescopes operating in the last decade (e.g., Albert et al. 2024; Aartsen et al. 2019), but these mostly concern neutrino alerts transmitted in the case of events clustering in space and time (two or more muon neutrino candidates in directional coincidence and arriving within a predefined time window), rather than starting from an X-ray/O transient.



In the specific case under investigation, the electromagnetic counterpart might arise from the UV and O cooling emission after SBO phenomena in CCSNe. In this regards, it is worth noticing that, contrarily to O wavelengths, the UV band is not well covered by currently operating instruments. This shortage will soon be mitigated by the launch of a new satellite sensible to the near-UV (NUV) band, named Ultraviolet Transient Astronomy Satellite (ULTRASAT) (Shvartzvald et al. 2023), planned for 2026. ULTRASAT will carry a UV telescope with an unprecedentedly field of view (FoV) of  $204 \text{ deg}^2$ . For comparison, the celestial volume monitored by ULTRASAT will be over 300 times that of GALEX. It will be able to detect emission in the near-UV band (230-290) nm, reaching a mean limiting magnitude of  $m_{\text{AB}}^{\text{lim,USAT}} = 22.5$  after 900 s of observation time at a statistical significance of  $5\sigma$ <sup>1</sup>. In this work, we quantify the improvement that the scientific community will gather once ULTRASAT will be operational, by combing its results with those of other existing facilities, as the Zwicky Transient Facility (ZTF) for the O band. The latter has been surveying the Northern sky since June of 2018 every 2-3 nights in g-band at (370-560) nm and r-band at (550-740) nm filters, while the i-band filter at (690-895) nm is used for partnership observations only. Note that ZTF is characterized by an instantaneous FoV of  $\sim 47 \text{ deg}^2$ , that represents the largest instantaneous field-of-view of any camera on a telescope of aperture greater than 0.5 m. In the following we will consider its  $5\sigma$  median sensitivity over all filters (g, r, and i bands) and all lunar phases for 30 seconds exposure, i.e.,  $m_{\text{AB}}^{\text{lim,ZTF}} = 20.4$  (Bellm et al. 2019). As at the moment of writing the ZTF future is still uncertain, namely it is unclear whether it will be operational<sup>2</sup> ULTRASAT launch, the results obtained and discussed throughout the manuscript in terms of ZTF have to be intended as related to ZTF-like instruments. In fact, our results are intended to provide a guidance to the scientific community for future MM studies involving  $\nu$ s, UV, and O signals. As such, in Section 3.1 we explain the methodology adopted to estimate the detectability of shock cooling UV and O emission from choked jets with ULTRASAT and ZTF, while in Section 3.2 we report the corresponding results.

### 3.1. Shock cooling emission from choked jets: detectability with ULTRASAT and ZTF

Starting from a set of fiducial progenitor parameters for BSGs and RSGs, we estimate the feasibility of combined observations between ULTRASAT and ZTF, in order to quantify the expected improvement in discovering signals from the shock cooling emission of choked-jet Type II SNe. We hence proceed to the comparison among available instrument responses and the model expectations about the specific intensity emissions resulting from SBOs as described in Equation (3). For RSGs we adopt progenitor parameters directly constrained from Type II SN observations. In particular, we start from the analysis in Ganot et al. (2022) relative to a sample of CCSN light curves characterized by clear NUV flares and optical detection in the R band, from simultaneous GALEX and Palomar Transient Factory (PTF) (Law et al. 2009; Rau et al. 2009) measurements between 24 May 2012 and 28 July 2012. In Ganot et al. (2022), the SN sample was fitted with the same model as the one considered in the present work, hence by averaging the best-fit values of Ganot

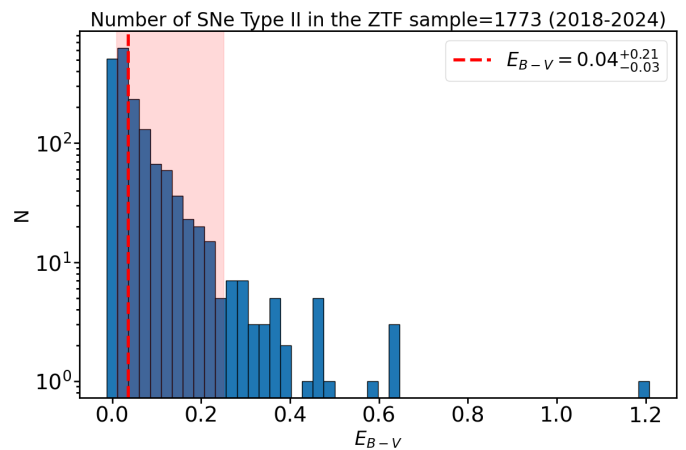


**Fig. 1.** Distribution of Galactic extinction values for galaxies hosting Type II SNe detected by ZTF (catalog available online in <https://sites.astro.caltech.edu/ztf/bts>). The used sample contains 1773 Type II SNe available in the ZTF Bright Transient Survey between June 2018 and the moment of writing (mid-February 2024). The dashed red line and the corresponding shaded region represent the median value of the distribution and the  $2\sigma$  uncertainty band, obtained via the 2.28th and 97.72nd percentiles.

et al. (2022) analysis, we obtain the following values, that we adopt as representative of the RSG population:  $R_* = 722 R_\odot$ ,  $E = 10^{51} \text{ erg}$ ,  $M_{\text{ej}} = 2.8 M_\odot$ , and  $f_\rho = 1.455$ . Note that these parameters are in agreement with theoretical and computational predictions (e.g., Goldberg & Bildsten 2020). For BSGs, in turn, we rely on modelling expectations, because these sources are still unconstrained by observations. Typical parameters for BSGs, that we set as representative of this population of sources, are:  $R_* = 50 R_\odot$ ,  $M_{\text{ej}} = 10 M_\odot$ ,  $f_\rho = 0.0465$ , and  $E = 10^{51} \text{ erg}$  (e.g., Dessart & Hillier 2019). For completeness, in Appendix A, we investigate the impact of these parameters on the model expected signals.

With regards to the extinction term in Equation (3), our analysis include its dependence on wavelength in order to properly predict the observable UV/O fluxes. In other words, we consider how the total extinction value varies with the wavelength  $\lambda$ , i.e.,  $A_\lambda = 1.086\tau_\lambda$ , rather than using a constant value. This choice is motivated by the fact that the extinction is very pronounced at UV wavelengths, being characterized by a bump at 220 nm, close to the ULTRASAT observational band. The total extinction in the visual V band is defined as  $A_V = R_V E_{B-V}$ , where  $E_{B-V} = E_{B-V}^{\text{observed}} - E_{B-V}^{\text{intrinsic}}$  represents the observed color excess and  $R_V$  is a parameter which characterizes the interstellar extinction from the near-infrared to the far-UV spectral region. We adopt the averaged dust extinction model of Cardelli et al. (1989) for diffuse interstellar medium in the Milky Way with  $R_V = 3.1$  from  $\lambda_{\text{min}} = 0.1 \mu\text{m}$  to  $\lambda_{\text{max}} = 3.3 \mu\text{m}$ . To realistically quantify the impact of extinction in our calculations, we use public data available from the ZTF Bright Transient Survey (BTS)<sup>3</sup>. By selecting the SN Type II reported in the catalog, we compute the median value of Galactic extinction characteristic of galaxies hosting the Type II SNe observed so far by ZTF. At the moment of writing, the sample contains 1773 sources classified as SN II, for a median extinction in their host galaxies of  $E_{B-V} = 0.04^{+0.21}_{-0.03}$  (see Figure 1). Therefore, we will consider the median  $E_{B-V} = 0.04$  as benchmark value in the follow-

<sup>1</sup> In the central  $170 \text{ deg}^2$  of the FoV and for a BB source of  $T_{\text{col}} = 20000 \text{ K}$ .

<sup>2</sup> The current program, in fact, will end in September 2024, see <https://www.ztf.caltech.edu/index.html> by the time of

<sup>3</sup> The sample is updated daily; results are available in <https://sites.astro.caltech.edu/ztf/bts>.

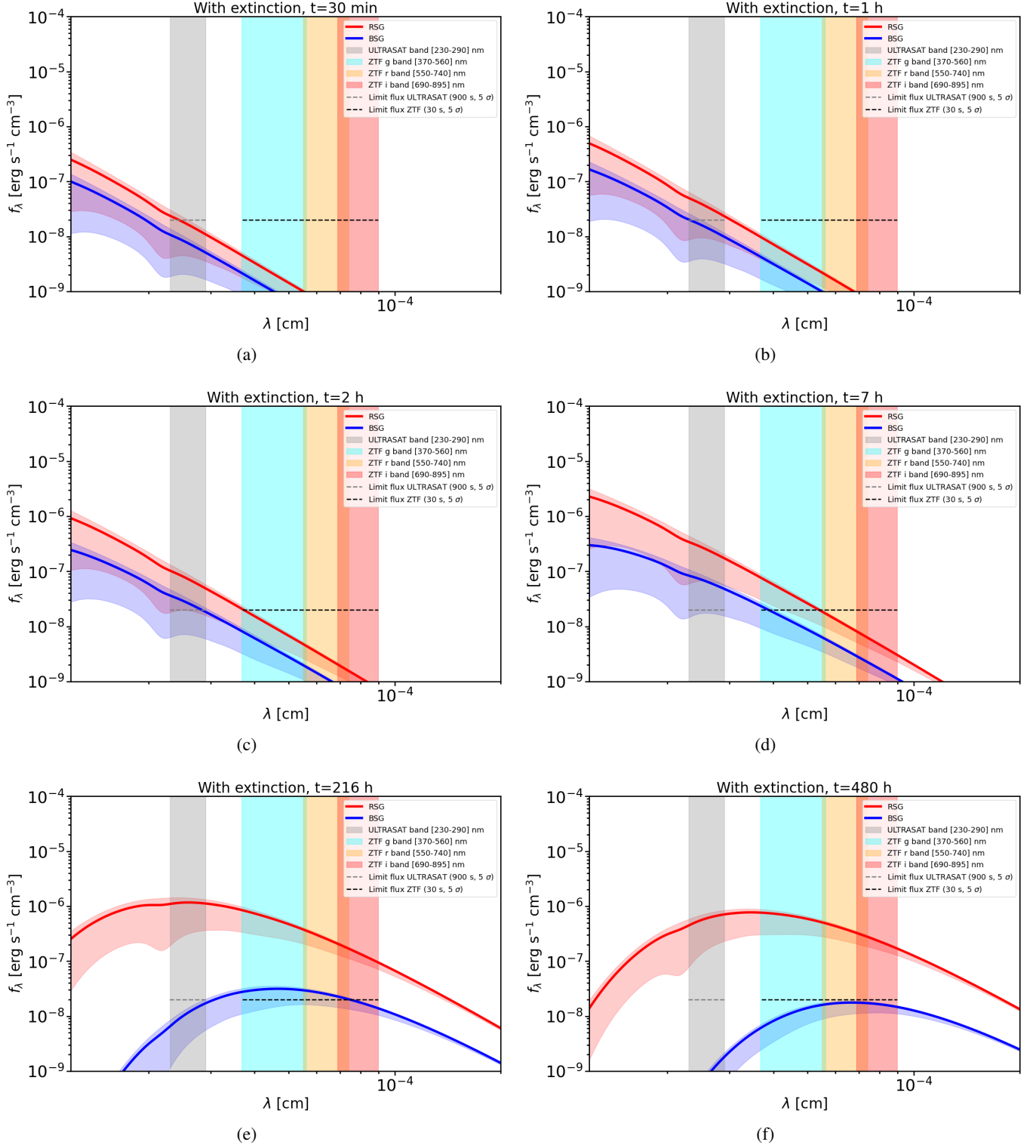


**Fig. 2.** Extinction-corrected specific intensities  $f_\lambda$  observable at Earth from a RSG (in red) and BSG (in blue) located at  $z = 0.01$ , as expected from the model in Equation (3). As input of the computation, fiducial parameters are used: for RSGs  $R_* = 722 R_\odot$ ,  $E = 10^{51}$  erg,  $M_{\text{ej}} = 2.8 M_\odot$ , and  $f_\rho = 1.455$ ; for BSGs  $R_* = 50 R_\odot$ ,  $M_{\text{ej}} = 10 M_\odot$ ,  $f_\rho = 0.0465$ , and  $E = 10^{51}$  erg. The solid lines show the expected emission with the median Galactic extinction  $E_{B-V} = 0.04$ , and the corresponding shaded region scans within the minimum and maximum extinction values, i.e.,  $E_{B-V} = 0.01$  and  $E_{B-V} = 0.25$ , respectively (see Figure 1). Vertical shaded bands represent the wavelength range covered by each instrument: ULTRASAT (in grey), and ZTF with  $g$  filter (in cyan),  $r$  filter (in yellow), and  $i$  filter (in red). The grey and black dashed horizontal lines define  $f_\lambda^{\text{lim}}$  of the two instruments, obtained following Equation (7). Panels from (a) to (f) refer to different evolution times, from 30 minutes to 20 days after the SBO event, highlighting for each stellar progenitor the time range when the emission becomes visible to ULTRASAT and ZTF.

ing evaluations, eventually including an uncertainty at  $2\sigma$  with  $E_{B-V} = 0.01$  and  $E_{B-V} = 0.25$  for the minimum and maximum extinction models presented in the following.

After correcting for extinction, we are ready to investigate the possible detectability of the estimated cooling emission signals from SBOs, by comparing them to the sensitivity of each instrument expressed as limiting magnitude in the AB system  $m_{AB}^{\text{lim}}$ . This is related to the minimum observable flux spectral density via the relation:

$$m_{AB} = -2.5 \log_{10} \left( \frac{f_\nu}{[\text{Jy}]} \right) + 8.90, \quad (6)$$

that can in turn be converted into the corresponding spectral flux density per unit wavelength  $f_\lambda$  as:

$$\frac{f_\nu}{[\text{Jy}]} = 3.34 \times 10^4 \left( \frac{\lambda}{\text{\AA}} \right)^2 \frac{f_\lambda}{[\text{erg cm}^{-2} \text{ s}^{-1} \text{ \AA}^{-1}]}, \quad (7)$$

where  $\lambda$  is the so-called *pivot* wavelength, i.e. the measure of the effective wavelength of a filter. For ULTRASAT we consider the average wavelength in its observational band ( $\bar{\lambda} = 260$  nm), while for ZTF we directly use value from the SVO Filter Provide Service<sup>4</sup> (Rodrigo et al. 2012; Rodrigo & Solano 2020). For both instruments we obtain  $f_\lambda^{\text{lim}} \approx 2 \times 10^{-8} \text{ erg cm}^{-2} \text{ s}^{-1}$ .

Figure 2 shows the expected extinction-corrected  $f_\lambda$  at different times after the SBO occurrence, as a result of the interaction between the cocoon embedding the choked jet and the stellar envelope of RSG/BSG stars. Here, a median redshift of  $z = 0.01$  (luminosity distance of about 40 Mpc) was set, in agreement with that where CCSNe are typically observed (e.g. Taggart & Perley (2021)). The figure also shows  $f_{\lambda, \text{USAT}}^{\text{lim}}$ ,  $f_{\lambda, \text{ZTF}}^{\text{lim}}$ , and the instrument's observation bands. These results suggest that, for representative RSGs and BSGs in an ambient medium with similar dust properties as our Galaxy, the UV emission from the SBO of RSGs(BSGs) would start to be visible by ULTRASAT ~30 minutes(1 hour) later. After at least 2(7) hours, RSG(BSG) emission might be detected also by ZTF. While the signal from RSG remains visible for the subsequent months both in O and UV bands, the one from BSGs is expected to last just ~8(18) days, when it goes below the ULTRASAT(ZTF) detection threshold. Apparently, the much larger progenitor radius of RSG stars leads the UV and O emission to remain widely visible for much longer as a result of the reduced cooling from expansion. Due to the strongly asymmetric distribution of  $E_{B-V}$  shown in Fig. 1, results obtained with the minimum and median extinction values are comparable. On the contrary, for the highest value of  $E_{B-V}$  in the  $2\sigma$  range: (i) the emission from RSGs(BSGs) becomes visible ~1.5(7) hours after the SBO; (ii) BSGs remain visible for ULTRASAT 3 days, while they cannot be detected by ZTF. Our results are consistent with results from current instruments, struggling to reveal CCSNe associated with BSG stars. In this regard, the role of ULTRASAT will be key for improving the capability of detecting this kind of sources, at least for the closest ones. Unfortunately, as side effect of the light absorption along the line of sight, the expected shape of the emission is more attenuated in correspondence of the ULTRASAT observational band, because of the bump at 220 nm characteristic of the extinction curve (Cardelli et al. 1989), as well visible in the spectral dips in Fig. 2.

We remark that, in the present work, we focused on the UV/O emission signal occurring on a timescale of days after the SBO.

<sup>4</sup> <http://svo2.cab.inta-csic.es/svo/theory/fps/>

In principle, similar investigations can be conducted concerning the UV detectability of the SBO flash that forms when the shock reaches the edge of the star. This signal would be visible as a pronounced peak in X-ray/UV wavelengths right after the SBO occurrence, on timescales ranging from seconds to a fraction of an hour. However, as for ULTRASAT the available limiting magnitude only refers to sources with a color temperature of  $T_{\text{col}} = 20,000$  K, which does not correctly describe the early emission phases, we postpone the investigation of X-ray/UV flashes to a future study. Indeed, for timescales shorter than 1 day, the color temperature is related to the photospheric temperature through  $T_{\text{col}} \approx 1.2T_{\text{ph}}$  (Rabinak & Waxman 2011), such that behind the shock wave  $T_{\text{col}}$  might reach  $\sim 10^5 - 10^6$  K.

### 3.2. Computation of rate of events

Following the arguments discussed in Section 3.1, we here calculate the rate of events per year  $\dot{N}$  expected to be detected into the instruments FoV as a function of the time  $t$  after the SBO occurrence, as below

$$\forall t \rightarrow \dot{N} = \int d\Omega \int_0^{z_{\text{lim}}} \frac{dN(z)}{dz} dz = \int d\Omega \int_0^{z_{\text{lim}}} \frac{R(z)}{1+z} \frac{dV(z)}{dz} dz, \quad (8)$$

where  $z_{\text{lim}}$  is the maximum  $z$  at which the model expected  $f_\lambda > f_\lambda^{\text{lim}}$  at given  $t$ . In the previous equation,  $dV(z)/dz$  is the differential comoving volume,  $R(z)$  is the comoving rate of sources, and  $1+z$  comes from the cosmological time dilation of the observed rate. The comoving rate can be expressed as

$$R(z) = R_0 \frac{(1+z)^{2.7}}{1 + \left( \frac{1+z}{2.9} \right)^{5.6}}, \quad (9)$$

being  $R_0 = 0.62 \times 10^{-4} \text{ Mpc}^{-3} \text{ yr}^{-1}$  the estimated local rate of Type II SNe (Li et al. 2011), and the redshift dependence follows the star formation rate from Madau & Dickinson (2014). In the present calculations we adopt the following assumptions:

- (i) as Type II SNe typically result from both RSG and BSG stars, while the ratio between BSGs and RSGs in our Galaxy is estimated to be  $\text{BSG/RSG} \approx 3$  on average (Eggenberger et al. 2002), we adopt as local rate for RSGs(BSGs)  $R_0 = 2.1(4.1) \times 10^{-5} \text{ Mpc}^{-3} \text{ yr}^{-1}$ ;
- (ii) in order to directly compare detector performances, we set the observation time of each instrument to 1 hour. In such a time, ZTF can scan  $3750 \text{ deg}^2$  of the sky (Bellm et al. 2019), while for ULTRASAT we conceive an observational strategy of  $4 \times 900 \text{ s}$ , each covering the ULTRASAT FoV =  $204 \text{ deg}^2$  (Shvartzvald et al. 2023). However, the source detection efficiency also depends on the instrument's duty cycle. For ULTRASAT it amounts to 100%, while for ZTF we consider just 25% of the rate of detectable sources as a result of the fact that ZTF can only operate nightly in good weather conditions (Dekany et al. 2020). To characterize RSG and BSG populations, we assume the same progenitor parameters as in Section 2 with median extinction equal to  $E_{B-V} = 0.04$ , since it is the value that best characterizes the Type II SN source population. Indeed, Equation (8) implicitly assumes that all Type II SNe entering into the calculation are characterized by the same  $E_{B-V}$  ( $z_{\text{lim}}$  is calculated for a fixed  $E_{B-V}$  value).

As a result, Figure 3a shows the maximum redshift as a function of the elapsed time since the SBO from which the signal can be revealed by ULTRASAT and ZTF. The trend shows a growing



horizon for a few days after the SBO (depending on the observing instrument), later decreasing, which reflects the presence of a peak of visibility in the emission : at later times, only closer sources can be still accessible. We also note that ULTRASAT will exploit larger volumes of the Universe for these explosions, being able to catch observations from farther redshifts. Figure 3b shows the corresponding number of Type II SNe per year detectable by ULTRASAT and ZTF (following Equation (8)) under the present assumptions.

## 4. Results and MM implications

In this Section, we discuss our results within the context of MM observations, focusing at first on UV and O electromagnetic signals visible by ULTRASAT and ZTF in Section 4.1, and later on neutrino associations in Section 4.2.

### 4.1. Ultraviolet and optical follow-ups

Figure 3a enables us to derive the following conclusions, namely:

i) If choked jets are embedded in RSG progenitors, UV(O) signal from SBOs by ULTRASAT(ZTF) can be detected out to  $z \sim 0.08(0.06)$ , corresponding to luminosity distances of  $\sim 360(270)$  Mpc, if the SBO occurred  $\sim 4(10)$  days before detections. Later emissions, as well as signals from times closer to the SBO, can still exceed the sensitivity of the detectors only for closer Type II SNe.

ii) If choked jets are embedded in BSG progenitors, the probability of detecting a analogous signal is smaller than RSGs because of the different stellar envelopes resulting into a weaker emission, as discussed in Section 3.1. In particular, ULTRASAT(ZTF) can detect SBO signals from BSGs located up to  $z \sim 0.023(0.017)$ , i.e., from luminosity distances of  $\sim 100(75)$  Mpc. About ten days after the SBO, the signal from BSGs is not visible anymore, unlike the one from RSGs that is instead detectable for several weeks. Furthermore, we highlight that our predictions about the maximum redshift reachable by ZTF are consistent with published results about the ZTF SN sample, whose public survey probes Type II SNe out to approximately  $z < 0.05$  (Perley et al. 2020).

These results are expected to help the scientific community in constraining the progenitor of Type II SNe observed in both UV and O wavelengths via ULTRASAT and ZTF-like instruments, as well as in identifying possible choked jets taking advantage of a multi-wavelength strategy. In fact, if the UV/O emission lasts more than ten days, this may indicate that such a choked jet was embedded in a RSG star. Moreover, the lack of a  $\gamma$ -ray counterpart (i.e., the associated GRB) points towards the observed emission to come from a choked jet, given that successful GRBs exploded at the distances here discussed are typically detected by current instruments. Note that missing  $\gamma$  rays can also result from off-axis GRBs that, despite of the presence of a successful jet, do not point directly towards Earth, hence their beamed emission would not be detected. However, their SBO emission is expected to last much less than what considered in this work. For large viewing angle models, in fact, the SBO luminosity suddenly reaches the peak value and declines. In other words, if UV and O emissions are detected over several days, it is reasonable to think that such signals are not related to off-axis GRBs (Suzuki & Shigeyama 2010).

Figure 3b shows the expected rate of detectable type II SNe as a function of time after the SBO event. It is visible that, once

ULTRASAT will be operational, the MM and multi-wavelength community can profit from at least as many observations as in the O field, or even more. Under the present assumptions, ULTRASAT will be able to reveal up to  $\sim 65(3)$  Type II SNe per year from RSGs(BSGs) if the detection is performed within  $\sim 4(1)$  day(s) after the SBO. About 60% of Type II SNe from RSGs can be accompanied also by an optical detection by ZTF, in case it will be able to catch O emission within  $\sim 10$  days after the SBO (namely, around one week after the UV one). Indeed, as already pointed out in Figure 3a, ZTF cannot perform sky observations as deep as ULTRASAT. As regards to the signals produced by BSG progenitors, one source out of the three detectable by ULTRASAT per year might be associated with O measurements by ZTF.

The results presented here can be influenced by specifics observational survey strategies implemented by the two instruments. Indeed, any real survey does not cover the whole sky, operates over a finite time window with a complex cadence structure, must contend with different values of Galactic extinction, and does not recover all of the transients it is able in principle to detect because of experimental selection criteria. More in details, the limiting magnitudes reachable by detectors change with the exposure time (the higher the latter, the lower the minimum flux detectable by each instrument). Additionally, while ULTRASAT will observe a large patch of the sky in both Southern and Northern hemispheres, ZTF scans declination values above  $-30^\circ$  ( $\sim 3\pi$  of the sky). In the light of this, we encourage the optimization of combined observations from different collaborations for a well-defined follow-up strategy tuned upon the results presented in this manuscript.

Within the MM context, neutrinos can also play a crucial role. Indeed, interaction of accelerated protons and thermal photons and/or hadronic collisions in choked jets can lead to the production of  $\nu$ s, able to escape from the thick stellar envelope of the system. This scenario has attracted much attention recently (e.g., Senno et al. 2016; Denton & Tamborra 2018; Guetta et al. 2020; Fasano et al. 2021), because of the possibility of explaining the astrophysical IceCube diffuse flux (TeV-PeV neutrino energies) without incurring into inconsistencies with isotropic diffuse  $\gamma$ -ray background observed by Fermi (e.g., Murase et al. 2016). In the next Section 4.2, we discuss how neutrino observations can be combined in association with electromagnetic signals from SBO events.

### 4.2. Neutrino follow-ups

During stellar collapse, neutrinos can escape the thickest envelopes, such that their detection would constitute an early warning for the MM astronomical community, advertising that the light from the explosion is coming. This would trigger the search for the SBO electromagnetic signals following core collapse. Therefore, the combination of MM signals from UV, O, and neutrino emissions provides an unprecedented opportunity to probe the existence of choked jets, and shed light on their progenitors.

High-energy neutrino telescopes, such as IceCube (Aartsen et al. 2017a) and KM3NeT (Adrián-Martínez et al. 2016), being this latter under construction at the bottom of the Mediterranean Sea and taking data in a partial detector configuration, may be able to reveal a flux of neutrinos from Type II SNe with choked jets, depending on their distance and energetics. Real-time analysis systems in these instruments allow for a prompt reaction, resulting into a distribution to the MM community within a few seconds. The high duty cycles of these instruments, combined with the all-sky field of view, make them ideal partners in MM

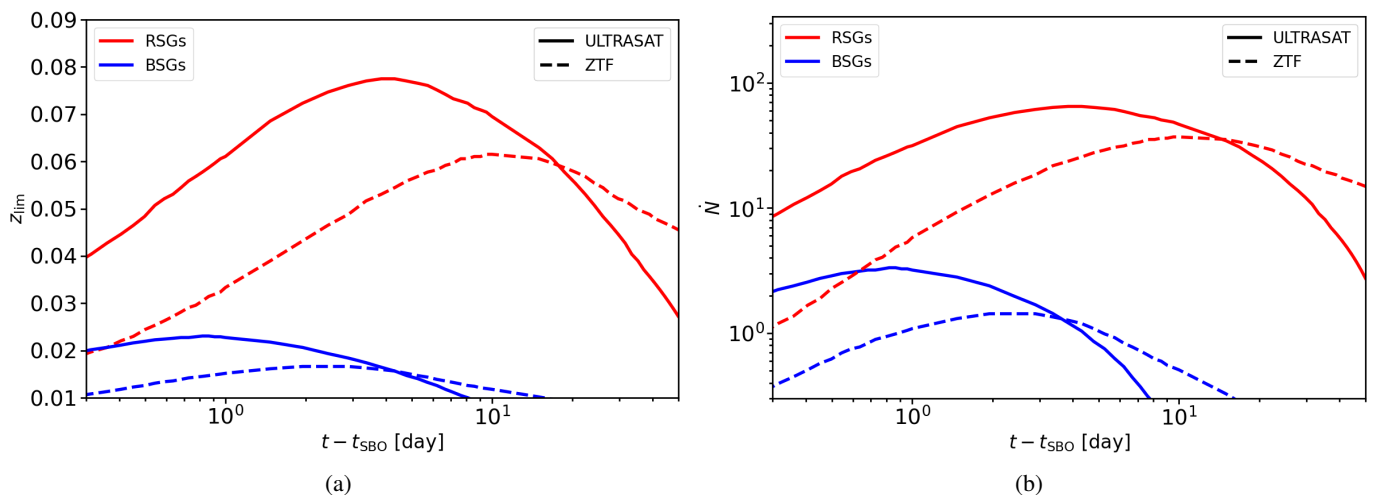


**Fig. 3.** (a) Maximum redshift from which RSGs and BSGs would have UV/O emissions detectable by ULTRASAT and ZTF as a function of the emission time  $t$ . (b) Rate of Type II SNe per year from RSGs and BSGs detectable with ULTRASAT and ZTF as a function of the emission time  $t$ . In both panels, the following fiducial parameters are adopted: for RSGs  $R_* = 722 R_\odot$ ,  $E = 10^{51}$  erg,  $M_{\text{ej}} = 2.8 M_\odot$ , and  $f_\rho = 1.455$ ; for BSGs  $R_* = 50 R_\odot$ ,  $M_{\text{ej}} = 10 M_\odot$ ,  $f_\rho = 0.0465$ , and  $E = 10^{51}$  erg. The emission time corresponds to the time elapsed since the SBO. Results for RSGs and BSGs are shown in red and blue, respectively. Solid and dashed lines are used for ULTRASAT and ZTF, respectively.

strategies. Note that IceCube has been sending neutrino alerts to external communities for triggering subsequent follow-ups since 2016 (Aartsen et al. 2017b), while for KM3NeT the plan is to automatically start sending alerts within the end of this year (see Celli et al. (2023) for the description about the current status of the KM3NeT online system). On the contrary, as regards the reception of external triggers, since November 2022 KM3NeT is reacting to any multi-messenger external alert via pipelines that automatically run analyses within time windows optimized to several classes of sources (Palacios Gonzalez et al. 2023). Instead, IceCube uses a Fast-Response Analysis (FRA) pipeline (Abbasi et al. 2021) that is manually activated to follow-up only selected interesting astrophysical transients.

We encourage UV, O, and neutrino telescopes to optimize both their alert sending and external follow-up strategy based on the results presented in this manuscript. By considering the maximal probability to detect Type II SNe (see Section 4), we can argue that, if an interesting neutrino alert is released, ULTRASAT(ZTF) could point to the suggested direction of the sky within around 4(10) days to search for possible electromagnetic counterparts, thus maximizing the reachable sky volume and hence the number of detectable sources. However, note that this time window leads to the time of the SBO occurrence. To also consider the production of neutrinos during the shock propagation time inside the stellar envelope, we need to enlarge this time window up to  $\sim 1$  day. In particular, we expect the shock wave to take  $\lesssim 1$  day to propagate in the radiative envelopes of BSGs and around 1 day in the convective envelopes of RSGs, for values of the explosion energy considered in this work (Kistler et al. 2013).

It is also worth pointing out that the approach presented in this paper (described in Section 3) can be extended to combined searches between any existent electromagnetic facility and neutrino telescopes. If a SN is detected somewhere in the Universe in UV and/or O wavelength band, by knowing its host galaxy (hence, its distance and the characteristic extinction) and by combining the information about the expected flux by the model and the limit flux detectable by the electromagnetic instrument reporting the detection, it is possible to define a reasonable time

window where looking for neutrinos coincident with different emission phases of that SN. E.g., the IceCube Collaboration has recently adopted this procedure in a FRA run with the aim of performing a search for track-like muon neutrino events arriving from the direction of the nearby Type II In SN 2024bch (Wiggins 2024; Balcon 2024) over two different time windows, in order to detect emission from either the shock propagation wave inside the stellar progenitor up to the shock breakout or the interaction of the ejecta with the circumstellar medium (Zegarelli et al. 2024). Because of no detections, upper limits on neutrino production from SN 2024bch were derived, under the simple assumption of a neutrino energy spectrum following an  $E^{-2}$  power law, as traditionally predicted by the Fermi shock acceleration (Fermi 1949).

Finally, our results can also be used to more accurately tune the neutrino search time window of offline analyses performed in correlation with observed SNe (Senno et al. 2018; Esmaili & Murase 2018). In fact, offline comprehensive studies might provide higher significance than real-time analyses via stacking sources from catalogs of O and UV emitters.

## 5. Summary and Conclusions

In this work, we investigated the radiative emission from choked jets embedded in CCSNe with extended hydrogen envelopes (Type II SNe), namely RSGs and BSGs. These sources are particularly interesting as their connection with GRBs indicates that these SN types can potentially host jets that are choked within the stellar envelopes. In the last decade, a few indications of the presence of jets in SNe have arisen. From the neutrino point of view, choked jets are extremely interesting as they are considered to be possible contributors to the astrophysical diffuse flux detected by IceCube.

Following the SBO occurrence, the stellar envelope expands and cools nearly adiabatically. As the photosphere penetrates into the outer shells of the envelope, radiation in the UV and O bands is emitted. We focused on this radiative signal, investigating future MM prospects for combined UV/O/neutrino observations between the future UV satellite ULTRASAT, the currently



operating optical telescope ZTF, and high-energy neutrino telescopes such as IceCube and KM3NeT. We follow the model by [Rabinak & Waxman \(2011\)](#) to estimate the expected photon flux, by considering fiducial values for stellar progenitor parameters:  $R_* = 722 R_\odot$ ,  $E = 10^{51}$  erg,  $M_{\text{ej}} = 2.8 M_\odot$ , and  $f_p = 1.455$  for RSGs, and  $R_* = 50 R_\odot$ ,  $E = 10^{51}$  erg,  $M_{\text{ej}} = 10 M_\odot$ , and  $f_p = 0.0465$  for BSGs. We then evaluated the possibility of detecting the extinction-corrected signals taking advantage of ULTRASAT for the UV band at (230-290) nm and the optical instrument ZTF. In this way, we characterized the future detection prospects of these sources, that we summarize in the following:

- If choked jets are embedded in RSG progenitors, the furthest UV(O) signal produced by the cooling emission after SBO can be detected by ULTRASAT(ZTF) up to  $z \sim 0.08(0.06)$ , or  $\sim 360(270)$  Mpc, if the SBO occurred  $\sim 4(10)$  days before detections. Lower-redshift SNe can still produce signals exceeding the limiting magnitude flux of the detectors even from later emission times or at times closer to the SBO.
- If choked jets are embedded in BSG progenitors, the probability of detecting a similar signal decreases with respect to RSGs because of the different characteristics among the two progenitors and subsequent less pronounced emission resulting from SBO in BSGs, as discussed in Section 3.1. In particular, ULTRASAT(ZTF) can detect signals coming from SBO occurred in BSGs located up to  $z \sim 0.023(0.017)$ , or  $\sim 100(75)$  Mpc.
- ULTRASAT will be able to reveal up to  $\sim 65(3)$  Type II SNe per year from RSGs(BSGs) if the detection is performed within  $\sim 4(1)$  days after the SBO.
- Around 60% of Type II SNe from RSGs can be accompanied also by an optical detection by ZTF, if it catches O emission within  $\sim 10$  days after the SBO (namely, around one week after the UV detection).
- One source out of the three detectable by ULTRASAT in one year in the case of Type II SNe from BSGs may be associated with optical measurement by ZTF.

As these sources can also produce neutrinos via interactions between protons and thermal photons in the choked jets, neutrino observations by existing Cherenkov high-energy neutrino telescopes (as IceCube and KM3NeT) can be used in association with electromagnetic signals coming from SBO events. Indeed, both IceCube and KM3NeT have leading roles into the MM community, working in synergy with several partners, in both offline and online analyses. In particular, much effort has been devoted to reconstructing and classifying their own data in real-time as to alert external communities about interesting neutrino events, as well as to follow-up interesting astrophysical transients revealed by other facilities. We find that:

- By considering the maximal probability to detect Type II SNe, if an interesting neutrino alert is released, under the hypothesis that it comes from the SBO emission phase, ULTRASAT(ZTF) could point to the provided direction of the sky within  $\sim 4(10)$  days to search for possible electromagnetic counterparts. In this way, the reachable sky volume is maximized, and hence the number of detectable sources.
- To consider the possibility that neutrinos are produced during the shock propagation time inside the stellar envelope, electromagnetic observations can wait up to a day more with respect to times indicated above.

Note that, besides fast follow-ups on single serendipitous sources (discussed in Section 4.2), the considerations presented

here can also be used for offline analyses based on the comparison between SNe catalogs and neutrino data. In fact, in these studies, the proper definition of the time window where searching for neutrinos is fundamental. Thanks to the results discussed here, we believe that the connection between choked jet SNe and high-energy cosmic neutrino can be more tightly constrained in the near future with respect to existing studies in the literature (e.g., [Senno et al. 2018](#); [Esmaili & Murase 2018](#)).

As already pointed out throughout the manuscript, at the moment of writing the ZTF program is planned to last up to September 2024 (ZTF-O4), and it is still unknown whether other runs in the future might overlap the ULTRASAT activity (whose launch is expected in 2026). Hence, all the results here discussed are to be interpreted in terms of ZTF-like instruments. Interestingly, the Large Array Survey Telescope (LAST), a multi-purpose telescope array in construction in the Israeli Negev Desert, will provide a great support to ULTRASAT, monitoring the Northern sky and providing simultaneous data in the visible wave band ([Ben-Ami et al. 2023](#); [Ofek et al. 2023](#)). LAST currently includes 32 out of 48 telescopes, and the deployment of the remaining telescopes is planned for mid-2023. In the future, optical surveys will be complemented also with measurements by the Large Synoptic Survey Telescope (LSST) at the Vera C. Rubin Observatory in Chile, that will observe the Southern sky ([Ivezić et al. 2019](#)). Preliminary estimations about the expected number of LSST detections for different SN progenitor types have been recently published in [Strothjohann et al. \(2024\)](#). Despite LSST will be characterized by higher performances than LAST (see Figure 1 in [Ofek et al. 2023](#) where the relative volume per unit time visible by several sky surveys is shown), LAST can provide follow-up observations for alerts that are not immediately observable by ZTF or LSST due to its geographic locations. In the light of this, we encourage future optical collaborations, as LAST and LSST, to take profit of our results for a proper definition of their alert streams strategy.

**Acknowledgements.** We acknowledge the support of the Sapienza School for Advanced Studies (SSAS) and the support of the Sapienza Grants No. RM120172AEF49A82, RG12117A87956C66 and RM1221816813FFA3. We gratefully acknowledge Antonio Capone for the useful discussions and comments to our work. We also thank Brad Cenko and Anna Franckowiak for the fruitful conversations and useful insights on the topics treated in the present paper. This work made use of Astropy:<sup>5</sup> a community-developed core Python package and an ecosystem of tools and resources for astronomy ([Astropy Collaboration et al. 2013, 2018, 2022](#)).

## References

- Aartsen, M. G., Abbasi, R., Abdou, Y., et al. 2013, *Phys. Rev. Lett.*, 111, 021103
- Aartsen, M. G., Ackermann, M., Adams, J., et al. 2019, *Phys. Rev. Lett.*, 122, 051102
- Aartsen, M. G., Ackermann, M., Adams, J., et al. 2017a, *Journal of Instrumentation*, 12, P03012
- Aartsen, M. G., Ackermann, M., Adams, J., et al. 2017b, *Astroparticle Physics*, 92, 30
- Abbasi, R., Ackermann, M., Adams, J., et al. 2021, *ApJ*, 910, 4
- Ackermann, M., Ajello, M., Albert, A., et al. 2015, *ApJ*, 799, 86
- Adrián-Martínez, S., Ageron, M., Aharonian, F., et al. 2016, *Journal of Physics G Nuclear Physics*, 43, 084001
- Albert, A., Alves, S., André, M., et al. 2024, *arXiv e-prints*, arXiv:2402.16498
- Arnett, W. D., Bahcall, J. N., Kirshner, R. P., & Woosley, S. E. 1989, *ARA&A*, 27, 629
- Astropy Collaboration, Price-Whelan, A. M., Lim, P. L., et al. 2022, *ApJ*, 935, 167
- Astropy Collaboration, Price-Whelan, A. M., Sipőcz, B. M., et al. 2018, *AJ*, 156, 123

<sup>5</sup> <http://www.astropy.org>

- Astropy Collaboration, Robitaille, T. P., Tollerud, E. J., et al. 2013, A&A, 558, A33
- Balcon, C. 2024, Transient Name Server Classification Report, 2024-284, 1
- Bartos, I., Dasgupta, B., & Márka, S. 2012, Phys. Rev. D, 86, 083007
- Bellm, E. C., Kulkarni, S. R., Graham, M. J., et al. 2019, PASP, 131, 018002
- Ben-Ami, S., Ofek, E. O., Polishook, D., et al. 2023, PASP, 135, 085002
- Bromberg, O., Nakar, E., Piran, T., & Sari, R. 2011, ApJ, 740, 100
- Cardelli, J. A., Clayton, G. C., & Mathis, J. S. 1989, ApJ, 345, 245
- Celli, S., Demin, P., Dornic, D., et al. 2023, PoS, ICRC2023, 1125
- Chang, P.-W., Zhou, B., Murase, K., & Kamionkowski, M. 2022, arXiv e-prints, arXiv:2210.03088
- Dekany, R., Smith, R. M., Riddle, R., et al. 2020, PASP, 132, 038001
- Denton, P. B. & Tamborra, I. 2018, ApJ, 855, 37
- Dessart, L. & Hillier, D. J. 2019, A&A, 622, A70
- Eggenberger, P., Meynet, G., & Maeder, A. 2002, A&A, 386, 576
- Esmaili, A. & Murase, K. 2018, J. Cosmology Astropart. Phys., 2018, 008
- Fasano, M., Celli, S., Guetta, D., et al. 2021, J. Cosmology Astropart. Phys., 2021, 044
- Fermi, E. 1949, Phys. Rev., 75, 1169
- Ganot, N., Gal-Yam, A., Ofek, E. O., et al. 2016, ApJ, 820, 57
- Ganot, N., Ofek, E. O., Gal-Yam, A., et al. 2022, ApJ, 931, 71
- Gehrels, N., Chincarini, G., Giommi, P., et al. 2004, ApJ, 611, 1005
- Gezari, S., Dessart, L., Basa, S., et al. 2008, ApJ, 683, L131
- Goldberg, J. A. & Bildsten, L. 2020, ApJ, 895, L45
- Guetta, D., Rahin, R., Bartos, I., & Della Valle, M. 2020, MNRAS, 492, 843
- He, H.-N., Kusenko, A., Nagataki, S., Fan, Y.-Z., & Wei, D.-M. 2018, ApJ, 856, 119
- Huang, F., Wang, X. F., Hosseinzadeh, G., et al. 2018, MNRAS, 475, 3959
- IceCube Collaboration. 2013, Science, 342, 1242856
- Ivezić, Ž., Kahn, S. M., Tyson, J. A., et al. 2019, ApJ, 873, 111
- Izzo, L., de Ugarte Postigo, A., Maeda, K., et al. 2019, Nature, 565, 324
- Kistler, M. D., Haxton, W. C., & Yüksel, H. 2013, ApJ, 778, 81
- Law, N. M., Kulkarni, S. R., Dekany, R. G., et al. 2009, PASP, 121, 1395
- Lazzati, D. & Begelman, M. C. 2005, ApJ, 629, 903
- Li, W., Chornock, R., Leaman, J., et al. 2011, MNRAS, 412, 1473
- MacFadyen, A. I. & Woosley, S. E. 1999, ApJ, 524, 262
- Madau, P. & Dickinson, M. 2014, ARA&A, 52, 415
- Matzner, C. D. 2003, MNRAS, 345, 575
- Mészáros, P. & Waxman, E. 2001, Phys. Rev. Lett., 87, 171102
- Modjaz, M., Li, W., Butler, N., et al. 2009, ApJ, 702, 226
- Murase, K., Guetta, D., & Ahlers, M. 2016, Phys. Rev. Lett., 116, 071101
- Nakar, E. & Piran, T. 2017, ApJ, 834, 28
- Nakar, E. & Sari, R. 2010, ApJ, 725, 904
- Nakauchi, D., Kashiyama, K., Suwa, Y., & Nakamura, T. 2013, ApJ, 778, 67
- Ofek, E. O., Ben-Ami, S., Polishook, D., et al. 2023, PASP, 135, 065001
- Palacios Gonzalez, J., Celli, S., Dornic, D., et al. 2023, PoS, ICRC2023, 1521
- Perley, D. A., Fremming, C., Sollerman, J., et al. 2020, ApJ, 904, 35
- Perna, R., Lazzati, D., & Cantiello, M. 2018, ApJ, 859, 48
- Pritchard, T. A., Roming, P. W. A., Brown, P. J., Bayless, A. J., & Frey, L. H. 2014, ApJ, 787, 157
- Quataert, E. & Kasen, D. 2012, MNRAS, 419, L1
- Rabinak, I. & Waxman, E. 2011, ApJ, 728, 63
- Rau, A., Kulkarni, S. R., Law, N. M., et al. 2009, PASP, 121, 1334
- Rodrigo, C. & Solano, E. 2020, in XIV.0 Scientific Meeting (virtual) of the Spanish Astronomical Society, 182
- Rodrigo, C., Solano, E., & Bayo, A. 2012, SVO Filter Profile Service Version 1.0, IVOA Working Draft 15 October 2012
- Roming, P., Pritchard, T., Brown, P., et al. 2010, in American Astronomical Society Meeting Abstracts, Vol. 215, American Astronomical Society Meeting Abstracts #215, 342.03
- Sapir, N., Katz, B., & Waxman, E. 2013, ApJ, 774, 79
- Senno, N., Murase, K., & Mészáros, P. 2016, Phys. Rev. D, 93, 083003
- Senno, N., Murase, K., & Mészáros, P. 2018, J. Cosmology Astropart. Phys., 2018, 025
- Shvartzvald, Y., Waxman, E., Gal-Yam, A., et al. 2023, arXiv e-prints, arXiv:2304.14482
- Strotjohann, N. L., Ofek, E. O., Gal-Yam, A., et al. 2024, ApJ, 960, 72
- Suzuki, A. & Shigeyama, T. 2010, ApJ, 717, L154
- Taggart, K. & Perley, D. A. 2021, MNRAS, 503, 3931
- Tamborra, I. & Murase, K. 2018, Space Sci. Rev., 214, 31
- Waxman, E. & Katz, B. 2017, in Handbook of Supernovae, ed. A. W. Alsabti & P. Murdin, 967
- Waxman, E., Mészáros, P., & Campana, S. 2007, ApJ, 667, 351
- Wiggins, P. 2024, Transient Name Server Discovery Report, 2024-281, 1
- Williams, B. F., Hillis, T. J., Murphy, J. W., et al. 2018, ApJ, 860, 39
- Woosley, S. E. & Bloom, J. S. 2006, ARA&A, 44, 507
- Wu, X.-F., Hou, S.-J., & Lei, W.-H. 2013, ApJ, 767, L36
- Zegarelli, A., Thwaites, J., Franckowiak, A., et al. 2024, The Astronomer's Telegram, 16443, 1

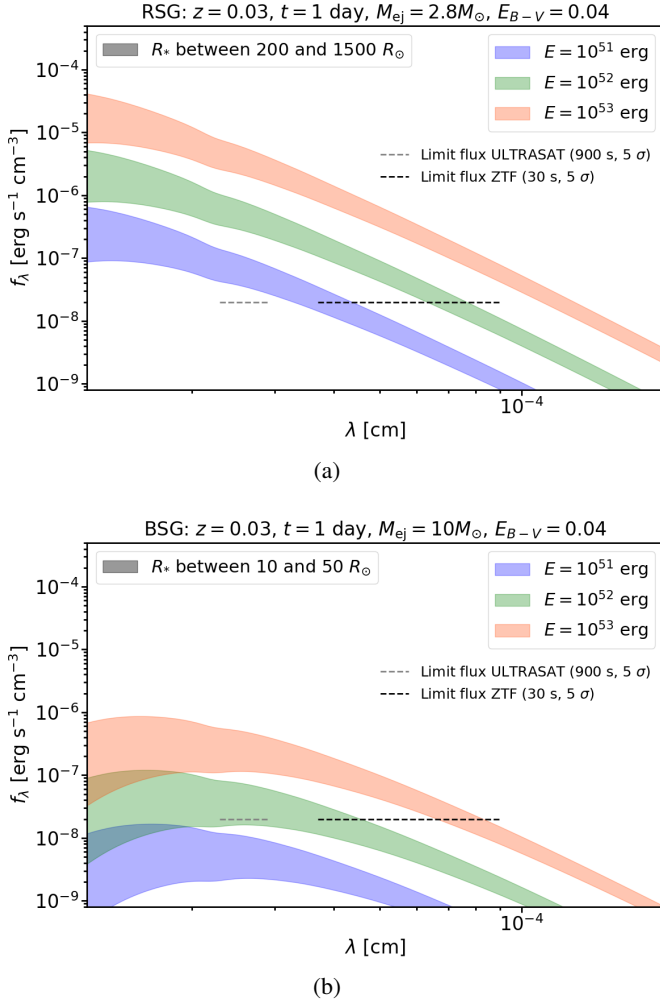


**Fig. A.1.** Model specific intensities  $f_\lambda$  (in Equation (3)) observed at Earth from RSGs (a) and BSGs (b) located at  $z = 0.03$  hosted in a galaxy with extinction value  $E_{B-V}$  (median value from Figure 1). Blue, green, and orange shaded regions show results for explosion energy  $E = 10^{51}$  erg,  $E = 10^{52}$  erg, and  $E = 10^{53}$  erg, respectively. (a) RSG progenitor: by fixing the ejected mass at  $M_{ej} = 2.8 M_\odot$  (fiducial parameter), the shaded regions reflect the variation of the progenitor radius between 200 and 1500  $R_\odot$ . (b) BSG progenitor: by fixing the ejected mass at  $M_{ej} = 10 M_\odot$  (fiducial parameter), the shaded regions reflect the variation of the progenitor radius between 10 and 50  $R_\odot$ .  $f_\lambda^{\text{lim}}$  of ULTRASAT and ZTF in their observational wavelength bands, obtained following Equation (7), are indicated with the grey and black dashed horizontal lines, respectively.

## Appendix A: Impact of the parameter space of the progenitors on the expected signals

In the present Section, we investigate how the radiative signal fluxes considered in this work are affected by the variation of parameters that characterizes the stellar progenitor. To this aim, we fix the value of Galactic extinction to  $E_{B-V} = 0.04$ , corresponding to the median extinction value for galaxies hosting SN Type II, as shown in Figure 1, the time of detection to 1 day after the SBO, and the redshift to  $z = 0.03$ . As discussed in Section 2.1, the radius and the effective temperature of the photosphere penetrating into the outer shells of the envelope in choked-jet systems directly influence the emissivity  $f_\lambda$  arising after the SBO (see Equation (3)), and these in turn are determined by stellar

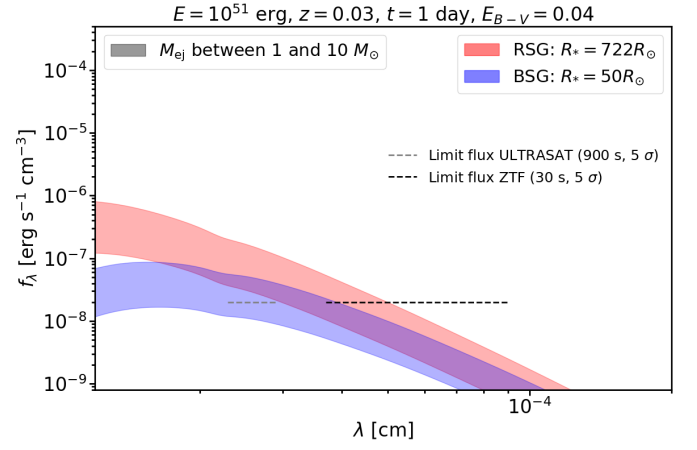


**Fig. A.2.** Model specific intensities  $f_\lambda$  (in Equation (3)) observed at Earth from RSGs (in red) and BSGs (in blue) located at  $z = 0.03$  hosted in a galaxy with extinction value  $E_{B-V}$  (median value from Figure 1). For each progenitor type, fiducial parameters are used (for RSGs  $R_* = 722 R_\odot$ ,  $E = 10^{51}$  erg, and  $f_p = 1.455$ ; for BSGs  $R_* = 50 R_\odot$ ,  $f_p = 0.0465$ , and  $E = 10^{51}$  erg), a part from the ejected mass  $M_{ej}$  that is let to vary between 1 and 10  $M_\odot$ .  $f_\lambda^{\text{lim}}$  of ULTRASAT and ZTF in their observational wavelength bands, obtained following Equation (7), are indicated with the grey and black dashed horizontal lines, respectively.

progenitor characteristics, namely by the stellar radius  $R_*$ , the explosion energy  $E$ , the ejected mass  $M_{ej}$ .

Throughout the work, we used fiducial parameters for both RSG and BSG progenitors. Here, we vary the stellar radii over ranges of possible parameters, namely  $[200-1500] R_\odot$  and  $[10-50] R_\odot$  for RSGs and BSGs, respectively, the ejecta mass values between 1 and 10  $M_\odot$ , and we also consider energies between  $10^{51}$  and  $10^{53}$  erg. Figure A.1 reports  $f_\lambda$  for different  $E$  and  $R_*$  within the aforementioned range of values. In particular, the left and right panel refer to RSG and BSG progenitors, respectively. In such a case, we adopt the fiducial  $M_{ej}$  values used previously in the manuscript. Clearly, (i) the higher the explosion and the larger the emission arising, and (ii) the more extended the stellar envelope and the higher the level of  $f_\lambda$ , because of the increasing amount of shocked material impacting the outer shell of the progenitor. This is more evident for RSG progenitors where  $r_{ph} \propto E_{51}^{0.41}$  and  $T_{ph} \propto E_{51}^{0.027}$ , while milder dependencies  $r_{ph} \propto E_{51}^{0.39}$  and  $T_{ph} \propto E_{51}^{0.016}$  characterize BSGs (see Equation (1) and Equation (2)). In Figure A.2, we fix the fiducial parameters for RSGs and BSGs, allowing the ejecta mass to vary between 1 and 10 solar masses: in such a case,  $f_\lambda$  is affected by less than a factor 10.